ELECTRON CLOUD INSTABILITY FOR A COASTING PROTON BEAM IN CIRCULAR ACCELERATORS

K. Ohmi *, T. Toyama, G. Rumolo[1]
KEK, 1-1 Oho, Tsukuba, 305-0801, Japan
[1]*GSI, Darmstadt, Germany*

Abstract

Instabilities for a coasting proton beam interacting with electron cloud are discussed. The electron sources are roughly classified into two categories reflecting their initial conditions: that is, the electrons produced at the chamber surface and/or at the beam position. If the beam is stable, it forms a Coulomb static potential around itself. Electrons produced near the beam position are trapped by the potential, while those produced at the chamber surface absorbed after once approaching the beam. We discuss the instability for the two cases in which electrons are produced at chamber and at beam position. The density of electrons are quite different according which initial condition. We notice that the production rate of electrons is important rather than the electron density.

INTRODUCTION

We study electron cloud instability for a coasting beam, in which the charged distribution is uniform along the longitudinal axis z. A static electric potential is formed by the coasting beam, when there is no transverse motion. We study the instability caused by electrons with two types of initial conditions: i.e., they produced at the beam position and at the chamber surface.

An energy of electron (E_e) is conserved for the interaction with a static coasting beam,

$$E_e = \frac{\boldsymbol{p}_\perp^2}{2m_e} + \frac{1}{2\epsilon_0}\frac{\lambda_p}{r} \tag{1}$$

where $\boldsymbol{p}_\perp$ and r are the transverse momentum and the distance from the beam, respectively, m_e the electron mass, and λ_p the line density of proton beam. The longitudinal motion of electrons is now neglected. Electrons created near the beam are trapped eternally, while electrons created at the chamber wall are absorbed into the wall after once approaching the beam with the same energy as those at the creation.

Electrons are created by ionization of the residual gas due to the proton beam. The electrons created near the beam are trapped and accumulated, with the result that their density could arrives a threshold of the ep instability. In this scenario, a coasting proton beam is always unstable. Above the threshold density, both of the beam and electron cloud become unstable. Considering transverse momentum conservation, it is conjectured that amplitudes of electrons are much larger than that of the beam. The electrons with a large amplitudes due to the instability are smeared by the nonlinear force due to the beam-electron interaction. The size of the electron cloud is enlarged, and electrons are absorbed into the chamber wall. Electrons are diffused by the instability, while the beam still could have a small oscillation amplitudes, with the result that the beam amplitude may be kept in the small level, and may be stable in actual operations of accelerators. We now take into account the production rate of electrons. Electrons are supplied successively with causing the instabiity, therefore the strength of the instability should be affected by the production rate.

Electrons are also created at the chamber wall surface due to proton beam loss and secondary electron. The electrons are not trapped by the coasting beam, if there is no perturbation. However the electron production rate at the wall is considered to be much higher than that due to ionization depending on the condition. It my be delicate problem which electrons, ionization or wall surface, is important for the instability. Beam perturbation, which acts as diffusion source for the trapped electron in the previous case, now acts as transition from nontrapping regime to trapping regime. This is the same physics in the meaning of the transition between the trapping and diffusion. The energy of the electrons is the order of 10 eV at the wall surface, except some portion with an energy equal to incident one. Therefore the multipacting is not developed naively in the coasting beam, because of keeping the initial energies. The beam with a perturbation traps the electrons created at the chamber during a short period or accelerates them to higher energy than initial one, then electrons are accumulated at a certain level, and the multipacting may be important even in the coasting beam.

In this situation discussed above, it seems to be difficult to understand the instability with a simple threshold formula given by linear theory. Detailed studies, which is taken into account the initial condition and production of electrons, were carried out in this work.

We summarize the production rates for the two initial conditions. Ionization cross-section for CO and H_2 is estimated to be $\sigma(\mathrm{CO}) = 1.3 \times 10^{-22}$ m^2 and $\sigma(\mathrm{H_2}) = 0.3 \times 10^{-22}$ m^2 using the Bethe formula [1]. The molecular density d_m is related to the partial pressure in nPa using the relation at 20 C, $d_m(\mathrm{m}^{-3}) = 2.4 \times 10^{11} P_m$ (nPa). The electron production rate is $7.7 \times 10^{-9} e^-/(\mathrm{m}\cdot p)$ at 2×10^{-7} Pa.

The electron production at the chamber wall is caused by hitting of beam particles, ions created by the beam, and electrons. The production rate, which depends on the accelerator design, could be much higher than ionization de-

* ohmi@post.kek.jp

pending on the condition or design of the ring. A proton with high energy and incidence of shallow angle create 100 electrons [2, 3], and an ion creates 10 electrons. For example, the proton loss and electron production rate are estimated to be 4×10^{-8} m^{-1} and $4 \times 10^{-6} e^-/(\mathrm{m}\cdot p)$, respectively, at PSR in LANL. Electrons are amplified by secondary electron emission.

We discuss the ep instability for the coasting beam caused by electrons due to the ionization and surface loss using computer simulations. Linear theory is reviewed in Sec. 2. The theory is based on the interaction between beam and trapped electrons. We use the theory as a criterion in varying degrees, though sufficient accuracy can not be expected for interaction during short period. More accurate discussion, which is related to beam stability and the electron diffusion, is presented by using a particle tracking method as is shown in Sec. 3. The simulation results are presented in Sec. 4 and 5 for ionization and particle loss, respectively.

LINEAR THEORY AND THRESHOLD OF THE INSTABILITY

We survey linear theory of ep instability [4], and estimate the threshold at some high intensity proton rings. It is convenient to survey status for many rings, apart from whether a sufficient accuracy can be expected to the linear theory.

The instability is characterized by the frequency of electron in the potential of the coasting beam,

$$\omega_e = \sqrt{\frac{\lambda_p r_e c^2}{2\sigma_{x(y)}(\sigma_x+\sigma_y)}}. \tag{2}$$

Landau damping, which is caused by the longitudinal slippage, is considered to be very strong, since the frequency is very rapid, $n \equiv \omega_e/\omega_0 \gg 1$.

The interactions between the beam and electron cloud is represented by a wake force [5]. The wake force is expressed by

$$W_1(z) = c\frac{R_S}{Q}\frac{\omega_e}{\tilde{\omega}} \exp\left(\frac{\alpha}{c}z\right) \sin\left(\frac{\tilde{\omega}}{c}z\right), \tag{3}$$

where

$$cR_S/Q = \frac{\lambda_e}{\lambda_p}\frac{L}{(\sigma_x+\sigma_y)\sigma_y}\frac{\omega_e}{c}. \tag{4}$$

in the language of impedance, we would say that the Q factor is infinite. Actually the frequency spread of ω_e should be taken into account. By taking into the frequency spread of ions, $\Delta\omega_e = \omega_e/2Q$, the impedance is given by

$$\begin{aligned} Z_1(\omega) &= \frac{c}{\omega}\frac{R_S}{1+iQ\left(\frac{\omega_e}{\omega}-\frac{\omega}{\omega_e}\right)} \\ &= \frac{\lambda_e}{\lambda_p}\frac{L}{\sigma_y(\sigma_x+\sigma_y)}\frac{\omega_e}{\omega}\frac{Z_0}{4\pi}\frac{Q}{1+iQ\left(\frac{\omega_e}{\omega}-\frac{\omega}{\omega_e}\right)}, \end{aligned} \tag{5}$$

where Z_0 is the vacuum impedance, $\sim 377\ \Omega$.

We discuss the stability of a beam which experiences the effective impedance. The stability criterion for the coasting beam is given by the dispersion relation as follows [6],

$$U \equiv \frac{\sqrt{3}\lambda_p r_p \beta\omega_0}{\gamma\omega_e\eta\sigma_E/E}\frac{|Z_1(\omega_e)|}{Z_0}, \tag{6}$$

where β is a typical value of the beta function in a ring, and r_p is the classical proton radius. This formula is the same as that given by Keil and Zotter for e-p instability [4]. For $U > 1$, the beam is unstable. The thresholds of the neutralization factor are given by

$$f_{th} = \frac{2\pi\gamma n\eta\sigma_E/E}{\sqrt{3}\lambda_p r_p \beta Q}\frac{\sigma_{x(y)}(\sigma_x+\sigma_y)}{L} \tag{7}$$

We put 5 and 10 m for Q and β, respectively, and the threshold values for various rings are shown in Table 1. The threshold values distribute wide range: i.e., rings with fast slippage have large values even for high intensity, while those with low slippage, large size of synchrotron, have low values.

SIMULATION USING BEAM TRACKING

We study the motion of proton beam interacting with the electron cloud using a tracking simulation. Simulation model is summarized as follows. A coasting proton beam is represented by macro-particles which are located along z with equal spacing. Each macro-particle has a charge and a mass corresponding to the proton line density. The macro-particle (proton) can undergo dipole motion with a dipole moment characterized by $\bar{\boldsymbol{x}}_{p,i}(z_i,s) = (\bar{x}_p, \bar{y}_p)$, but the emittance (size) is kept constant. The number of macro-protons should be more $\omega_e L/c$, because electrons in the cloud oscillate smoothly by the force from the macro-protons. The electron cloud is created at some positions in the ring, and is represented by a large number of point-like macro-particles denoted by $\boldsymbol{x}_{e,a}$ ($a = 1, N_e$). The electrons are created in every passage of the proton beam with the initial condition of adopted model: namely they are created at the beam position or at the chamber surface. The transverse position of electrons is randomly generated at the chamber center with the same rms size as the beam, or at the chamber surface uniformly along azimuthal angle.

The equations of motion of macro-protons and macro-electrons in cloud are expressed by

$$\frac{d^2\bar{\boldsymbol{x}}_{p,i}}{ds^2} + K(s)\bar{\boldsymbol{x}}_{p,i} = -\frac{2r_p}{\gamma}\sum_{a=1}^{N_e}\boldsymbol{F}_G(\bar{\boldsymbol{x}}_{p,i}-\boldsymbol{x}_{e,a};\boldsymbol{\sigma})\delta(s-s_e) \tag{8}$$

$$\frac{d^2\boldsymbol{x}_{e,a}}{dt^2} = -2r_e c\sum_{i=1}^{N_{sl}}\lambda_p(z_i)\Delta z\boldsymbol{F}_G(\boldsymbol{x}_{e,a}-\bar{\boldsymbol{x}}_{p,i};\boldsymbol{\sigma})\delta(t-t(z_i,s_e)). \tag{9}$$

The instability is simulated by solving these equations self-consistently.

Table 1: Basic parameters and threshold values of the neutralization factor of various proton rings

variable	symbol (unit)	JPARC-MR	KEK-PS	PSR	ISIS	AGS-Bst.	AGS	FNAL-MI
circumference	L (m)	1567.5	339	90	163	202	800	3319
relativistic factor	γ	54.	12.8	1.85	1.07	1.2	3.0	128
beam line density	$\lambda_p(\times 10^{10})$ m^{-1}	21.2	0.74	33.3	18.4	82.7	8.75	0.90
rms beam sizes	σ_r (cm)	0.35	0.5	1.0	3.8	1	0.7	0.17
rms energy spread	σ_E/E (%)	0.25	0.3	0.4	0.5	0.5	0.28	0.03
transition energy	γ_t	31.6 i	6.76	3.08	5.07	4.88	8.5	21.8
slippage factor	η	-0.0013	0.016	-0.187	-0.83	-0.652	0.0122	0.0020
	$\omega_e L/c$	7740	225	195	69	226	2012	6930
Threshold	$f_{th}(\%)$	0.21	4.0	2.5	45.	15.	2.6	0.06

Before going to beam tracking, we show electron motion trapped in the beam potential. The second equation, Eq. (9), is used for tracking electrons, where the proton coordinate $\bar{\boldsymbol{x}}_{p,i}$ is fixed or modulated with a frequency. Fig. 1 shows samples of electron trajectories for static beam potential and for including a perturbation due to a coherent motion of beam. Motion of three samples of electrons in a static potential are depicted in Fig. 1(a). It shows that electrons are trapped in the potential. Fig. 1(b) depicts motion of an electron in a perturbed potential. The proton beam with $\sigma_y = 5$ mm was modulated with amplitude of 1 mm and with frequency of 1.1 GHz. The amplitude of the electron gradually increase as time goes by. Detailed calculations with various proton amplitudes and various modulation frequency is seen in Ref. [7].

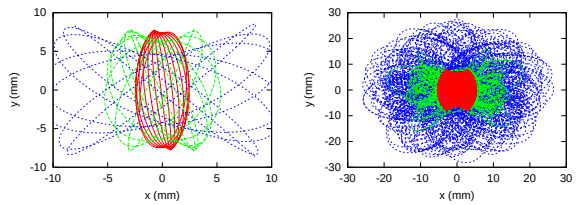

Figure 1: Trajectory of electrons. (a) Three electrons are tracked without perturbation. (b) An electrons are tracked with perturbation. Green and blue points are phase space coordinate of electron during 10 turns and 100 turns, respectively. Red points are those without perturbation as a reference.

The instability behavior is studied by solving the equations of protons and electrons, Eq. (8) and (9), simultaneously. The motion of the macro-electrons and macro-protons is tracked during the beam passage. After the interactions, macro-protons are transported by the lattice magnets. This procedure is repeated in every interaction of the bunch with the cloud. The number of macro-electrons increases except their disappear at the wall.

When electrons are absorbed at the chamber wall surface, secondary electron emission is taken into account with the formula,

$$\begin{aligned} \delta_2(E) &= \delta_2(0)\exp(-5E/E_{\max}) \\ &+ \delta_{2,\max} \times \frac{E}{E_{\max}} \frac{1.44}{0.44 + (E/E_{\max})^{1.44}}, \end{aligned} \tag{10}$$

where $E_{\max} = 200$ eV, $\delta_2(0) = 0.5$, and $\delta_{2,\max} = 2.1$.

We take into account the Landau damping caused by the longitudinal motion, which disturbs the coherence of the dipole motion. The Landau damping rate per one revolution is given by $\alpha = n\eta\sigma_E/E/\sqrt{3}$ for the coasting beam, where $n = \omega_e/\omega_0$. In this simulation, the Landau damping is treated by a simple way as

$$\bar{\boldsymbol{x}}_{p,i} = (1-\alpha)\bar{\boldsymbol{x}}_{p,i}. \tag{11}$$

We performed the simulation for J-PARC 50 GeV rings at the flat top. The damping rate is 1.1×10^{-3} from the parameter shown in Table 1.

We put 10 interaction points in the ring. The dipole motion of the beam is assumed to be periodic for each section divided into 1/10 part of the whole ring. In this model, the coasting beam (macro-proton train) with length of 1/10 of the circumference is tracked. The beam (1/10 part) is represented by 3000 macro-protons. Frequency of electrons or proton beam is limited by interval of the revolution frequency of 1/10 circumference due to the periodic condition. Considering the spread of the electron frequency, $n = \omega_e/\omega_0$ for the model has to be larger than Q. Since the quality factor of electron oscillation is not so high ~ 10, $n = 7740/20\pi = 123 \gg Q$ is satisfied. The number of macro-proton has to represent the oscillation of the coasting beam smoothly: namely, the number should be larger than n. The number of 3000 macro-protons satisfies the condition.

INSTABILITY DUE TO IONIZATION ELECTRON

We first discuss instability caused by electrons produced at the beam position, where electrons are considered to be produced by ionization. Increase of the neutralization factor per one revolution time (T_0) is estimated to be

$7.7 \times 10^{-9} e^-/(\mathrm{m}{\cdot}p) \times 1567 = 1.2 \times 10^{-5} T_0^{-1}$ for ionization at the vacuum pressure, $P = 2 \times 10^{-7}$ Pa. The build up time up to the threshold (0.21%) is 170 turns (0.9 ms) for this vacuum pressure. The production rate linearly depends on the vacuum pressure, therefore build-up time becomes faster increasing the pressure.

The simulations were performed for several electron production rates, at a range between $7.7 \times 10^{-9} \sim 7.7 \times 10^{-3}) e^-/(\mathrm{m}{\cdot}p)$, though the high values $> 10^{-6}$ corresponding vacuum pressure $> 10^{-5}$ Pa are impossible in an actual machine.

The simulation evaluated amplitudes of each macro-proton ($J_{x(y),i}$), electron line density (λ_e), electron rms. size (σ_e), etc. turn by turn. There was no significant result for the production rate of $7.7 \times 10^{-9} e^-/(\mathrm{m}{\cdot}p)$, correspond to $P = 2 \times 10^{-7}$ Pa. Figure 2 shows results for a production rate 10 times more, $7.7 \times 10^{-8} e^-/(\mathrm{m}{\cdot}p)$ ($P = 2 \times 10^{-6}$ Pa). The neutralization factor (λ_e/λ_p) in picture (a) linearly increase and is saturated at around 10 times higher density than the threshold. The maximum amplitude normalized by the beam size ($\sqrt{J_{x(y),i}/\varepsilon_{x(y)}}$ is depicted in picture (b). It grows up to 1% of the beam emittance and is saturated. Size of electron cloud σ_e, which is plotted in picture (c), is the same size as the beam at the initial stage and then starts to increase at around the density exceeds the threshold. The saturation level is determined by the chamber radius. Though the pictures showed instability feature, we may not observe the instability actually due to the small amplitude (1% of the size).

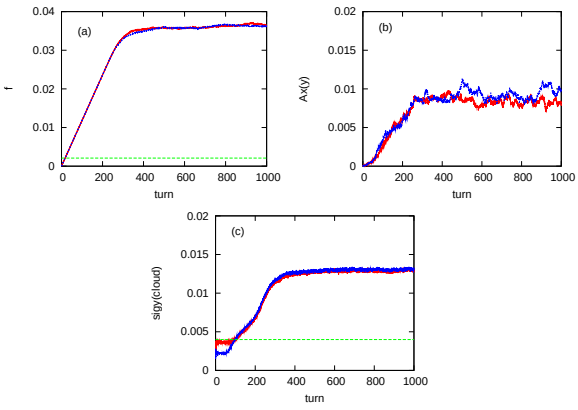

Figure 2: Evolution of neutralization factor for electron cloud, maximum normalized amplitude of beam ($(J_{x(y)}/\varepsilon_{x(y)})^{1/2}$) and size of electron cloud ($\sigma_{x(y)}$ [m]) for the eletron production rate of $7.7 \times 10^{-8} e^-/(\mathrm{m}{\cdot}p)$.

Figure 3 shows electron line density λ_e and maximum amplitude $\sqrt{J_{x(y)}}$ for higher electron production rates of 7.7×10^{-7}, 7.7×10^{-6} and $7.7 \times 10^{-5} e^-/(\mathrm{m}{\cdot}p)$. The rates are convereted vacuum pressure, $P = 2 \times 10^{-5}$, 2×10^{-4} and 2×10^{-3} Pa, respectively. Needless to say, the high vacuum pressure is nonsense for actual accelerators. Pictures (a), (c) and (e) are the electron line density for the production rates. The line density increases at the early stage, is saturated, then turn to decrease, and finally settle on a certain density. The final density is around 10^{10} m^{-1} independent of the production rate, and it is 20 times of the threshold in the linear theory. Two lines, which are depicted in the pictures, are given for the line density with or without secondary electron emission. There was no remarkable difference with or without secondary emission, except for the last picture (e). Picture (e) shows a sudden increase of the electron line density with secondary emission, which is caused by strong multipactoring. Pictures (b), (d) and (f) are evolutions of horizontal (red) and vertical (blue) amplitude for the production rates. The seconday emission is included. The amplitude is saturated at 3% of the beam size for the production rate of $7.7 \times 10^{-7} e^-/(\mathrm{m}{\cdot}p)$. The amplitudes for higher rates are not saturated as long as we simulated. σ_r/10 and σ_r, respectively. If we can observe the instabilities with a resolution of 10% of σ_r, the production rate should be more than $10^{-6} e^-/(\mathrm{m}{\cdot}p)$. which corresponds to 10^{-4} Pa. This value is too high for the vacuum pressure of accelerators. Picture (f) shows sudden increase of horizontal and vertical amplitudes, which correspond to the increase seen in picture (e). These pictures show that strong multipactoring is induced by the beam oscillation with an amplitude $1/3 \sim 1/2$.

The electron line density exceeds for every cases of various production rates. The instability behavior is determined by electron production rate rather than the fact whether the density exceeds the threshold value.

INSTABILITY DUE TO ELECTRONS FROM CHAMBER SURFACE

We understood that the production rate is important factor for the beam instability in previous section. The ionization electron for ordinary vacuum pressure was too low production rate to cause instability. Therefore we now consider the electrons produced at the chamber wall. The electron production at the wall is considered to be much higher than that of ionization. For production rate at the chamber surface, we consider $4 \times 10^{-6} e^-/(\mathrm{m}{\cdot}p)$ as a standard value. If electrons are created with this rate and are accumulated, the density arrives at the threshold level (0.21%) for traveling of proton beam of 1/3 turn, 525 m, 1.8 μsec. The time is not very short, but is rather long, if we consider the electron oscillation frequency, $f_e = \omega_e/2\pi = 4$ nsec.

Figure 4 shows electron line density and normalized beam amplitude for various production rate, 7.7×10^{-8}, 7.7×10^{-7}, 7.7×10^{-6} and $7.7 \times 10^{-5} e^-/(\mathrm{m}{\cdot}p)$. The beam instability is invisible for the lowest production rate, $7.7 \times 10^{-8} e^-/(\mathrm{m}{\cdot}p)$. The threshold density prediceted by linear theory is drawn by green lines in the pictures. The cloud density exceed the threshold for the rate, $7.7 \times 10^{-7} e^-/(\mathrm{m}{\cdot}p)$, but the amplitude grows up to only 1% of the beam size. For $7.7 \times 10^{-6} e^-/(\mathrm{m}{\cdot}p)$, the electron density reaches 5 times of the threshold and the amplitude grows 10% of the beam size. The amplitudes may be se-

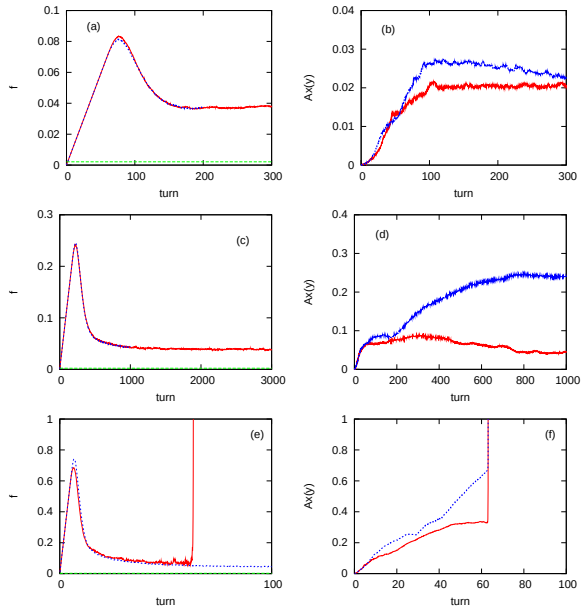

Figure 3: Evolution of neutralization factor for electron cloud and maximum normalized amplitude of beam ($\sqrt{J_{x(y)}/\varepsilon_{x(y)}}$) for various eletron production rates. Pictures (a), (c) and (e) are the electron line density for the production rates given for the line density with or without secondary electron emission. The threshold density given by linear theory is drawn by Green straight line. Pictures (b), (d) and (f) are evolutions of horizontal (red) and vertical (blue) amplitude. Pictures (a) and (b) are electron density and beam amplitudes for $7.7 \times 10^{-7} e^-/(\mathrm{m}{\cdot}p)$, (c) and (d) are for $7.7 \times 10^{-6} e^-/(\mathrm{m}{\cdot}p)$, and (e) and (f) are for $7.7 \times 10^{-5} e^-/(\mathrm{m}{\cdot}p)$.

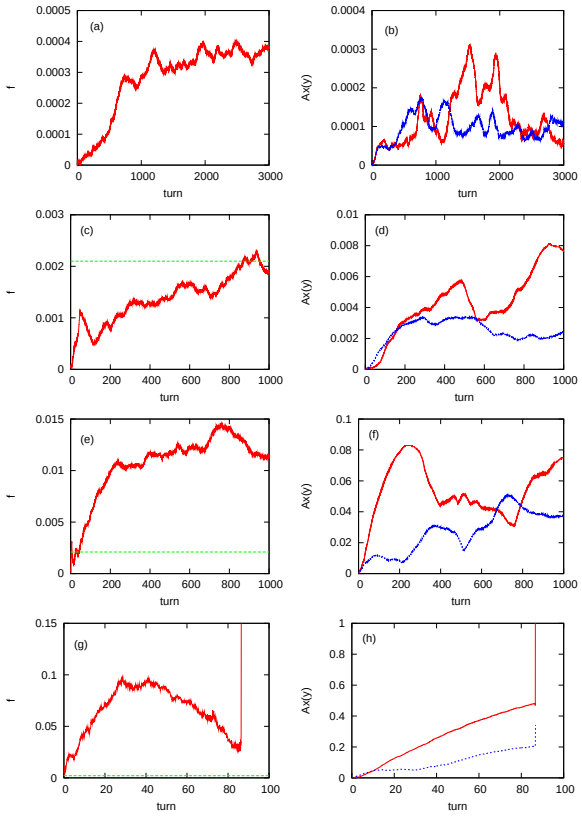

Figure 4: Evolution of neutralization factor for electron cloud and maximum normalized amplitude of beam ($\sqrt{J_{x(y)}/\varepsilon_{x(y)}}$) for various electron production rates. Pictures (a) and (b) are neutralization factor and beam amplitudes for 7.7×10^{-8}, (c) and (d) are for 7.7×10^{-7}, (e) and (f) are for 7.7×10^{-6}, and (g) and (h) are for $7.7 \times 10^{-5} e^-/(\mathrm{m}{\cdot}p)$. The threshold density given by linear theory is drawn by Green straight line in the pictures (a), (c), (e) and(g).

rious level for an actual operation. A sudden increase in the line density and amplitude, which is caused by electron multipactoring, was seen for $7.7 \times 10^{-5} e^-/(\mathrm{m}{\cdot}p)$ in pictures (g) and (h). The beam oscillation with an amplitude $\sim 1/3$ of the size induced the multipactoring again.

The electron production rate around $10^{-6} \sim 10^{-5}$ is critical for the instability at coasting beam operation in J-PARC main ring. If one proton loss produces 100 electrons, the proton loss rate should be reduced less than $10^{-8} \sim 10^{-7}/\mathrm{m}{\cdot}p)$.

CONCLUSION

Electron cloud instability for a coasting proton beam has been studied. We treated electrons which are created by ionization at the beam position and by beam particle loss and secondary emission at the chamber wall surface.

The electron cloud produced by ionization at the beam position can always exceeds the threshold given by linear theory, since they are trapped by the beam. The build-up time is fast ($\sim$ ms) in machines with especially low slippage factor, because of the low threshold neutralization factor. A simulation, in which the motion of beam and electrons was solved simultaneously, has been carried out to study the stability of the electron-proton system. The production rate more than $10^{-6} e^-/(\mathrm{m}{\cdot}p)$ was criteria to be unstable for JPARC-MR ring. The rate corresponds to 10^{-4} Pa, which is quite nonsense value for accelerators. Ionization may not be a direct candidate of the instability for the coasting beam.

Electron sources with a higher production rate, for example, proton loss and/or multipacting were paid attention. Since the electrons produced at the wall surface were not trapped by the coasting beam, they were not accumulated much, but were sufficient to cause the instability.

The simulation was applied for electrons produced at the wall. The beam amplitude grows to visible level due to the instability for the production rate, $10^{-6} e^-/(\mathrm{m}{\cdot}p)$. This value, which is the same as that given for ionization electrons, is now possible level for production due to proton loss in high intensity proton rings.

Production rate was important whether the instability grows to visible amplitudes. The electron production due to proton loss and/or multipacting have an essential role even for the coasting beam instability. The instability was not caused by electron cloud for slow production rate, $< 10^{-7} e^{-}/(\mathrm{m}{\cdot}p)$, for both cases.

We should to change our understanding for the threshold given by linear theory. The threshold was quite inconsistent for trapped electron, which was modeled in the linear theory. If anything, the threshold is rather consistent with the case of electrons produced at the wall. It was also consistent with the case of bunched beam model [5].

Similar analysis and discussion can be extended to the beam-ion instability in electron storage rings straightforwardly.

ACKNOWLEDGMENTS

The authors thank the members of the instability working group of J-PARC, N. Hayashi, F. Noda, S. Kato, K. Satoh, Y. Shobuda, S. Machida, K. Oide K. Yokoya for fruitful discussions.

REFERENCES

[1] Y. Baconnier, CERN report 85-19, pp.267 (1985).

[2] R. J. Macek, A. Browman, D. Fitzgerald, R. C. McCrady, F. E. Merrill, M. A. Plum, T. Spickermann, T.-S. Wang (LANL), K. C. Harkay, R. Kustom, R. A. Rosenberg (ANL), J. E. Griffin, K. Y. Ng and D. Wildman, Proceedings of Part. Accel. Conf. 2001, 688 (2001)

[3] M. A. Furman and M. Pivi, Proceedings of the 2001 Part. Accel. Conf., 2001, 707 (2001).

[4] E. Keil and B. Zotter, CERN-ISR-TH/71-58 (1971).

[5] K. Ohmi, T. Toyama, C. Ohmori, Phys. Rev. ST-AB.,**5**, 124402 (2002).

[6] E. Keil and W. Schnell, CERN Report TH-RF/69-48 (1969).

[7] G. Rumolo and K. Ohmi, KEK preprint 2003-94.